Characterization of the Formability of High-Purity Polycrystalline Niobium Sheets for Superconducting Radiofrequency Applications

Jean-François Croteau, Guillaume Robin, Elisa Cantergiani, Said Atieh, Nicolas Jacques, Gilles Mazars, Marion Martiny

Jean-François Croteau[1]
I-Cube Research/Bmax,
30 Boulevard de Thibaud,
Toulouse 31104, France;
ENSTA Bretagne,
UMR CNRS 6027, IRDL,
2 rue François Verny,
Brest Cedex 9 F-29806, France
e-mails: jean-francois.croteau@icube-research.com; jean-francois.croteau@ensta-bretagne.org

Guillaume Robin
Université de Lorraine, CNRS,
Arts et Métiers ParisTech, LEM3,
7 rue Félix Savart,
57070 Metz, France
e-mail: guillaume.robin@univ-lorraine.fr

Elisa Cantergiani
I-Cube Research/Bmax,
30 Boulevard de Thibaud,
Toulouse 31104, France
e-mail: elisa.cantergiani@icube-research.com

Said Atieh
European Organization for Nuclear Research (CERN),
Geneva 1211, Switzerland
e-mail: said.atieh@cern.ch

Nicolas Jacques
ENSTA Bretagne,
UMR CNRS 6027, IRDL,
2 rue François Verny,
Brest Cedex 9 F-29806, France
e-mail: nicolas.jacques@ensta-bretagne.fr

Gilles Mazars
I-Cube Research/Bmax,
30 Boulevard de Thibaud,
Toulouse 31104, France
e-mail: gilles.mazars@icube-research.com

Marion Martiny
Université de Lorraine, CNRS,
Arts et Métiers ParisTech, LEM3,
7 rue Félix Savart,
57070 Metz, France
e-mail: marion.martiny@univ-lorraine.fr

Characterization of the Formability of High-Purity Polycrystalline Niobium Sheets for Superconducting Radiofrequency Applications

The forming limit diagram (FLD) of high-purity niobium sheets used for the manufacturing of superconducting radiofrequency (SRF) cavities is presented. The Marciniak (in-plane) test was used with niobium blanks with a thickness of 1 mm and blank carriers of annealed oxygen-free electronic (OFE) copper. A high formability was measured, with an approximate true major strain at necking for plane strain of 0.44. The high formability of high-purity niobium is likely caused by its high strain rate sensitivity of 0.112. Plastic strain anisotropies (r-values) of 1.66, 1.00, and 2.30 were measured in the 0 deg, 45 deg, and 90 deg directions. However, stress–strain curves at a nominal strain rate of $\sim 10^{-3}$ s^{-1} showed similar mechanical properties in the three directions. Theoretical calculations of the forming limit curves (FLCs) were conducted using an analytical two-zone model. The obtained results indicate that the anisotropy and strain rate sensitivity of niobium affect its formability. The model was used to investigate the influence of strain rate on strains at necking. The obtained results suggest that the use of high-speed sheet forming should further increase the formability of niobium. [DOI: 10.1115/1.4052557]

Keywords: forming limit diagram, Marciniak test, two-zone model, niobium, SRF, mechanical behavior, metals, plastic behavior

1 Introduction

Sheet forming of complex high-purity niobium (with a residual resistivity ratio (RRR) greater than 300) superconducting radiofrequency (SRF) cavities like CERN's crab cavity [1] or high-β elliptical cavities [2] is crucial to increase the luminosity and the collision energy of future particle accelerators like the Future Circular Collider [3,4]. To optimize the sheet forming processes, e.g., deep-drawing, spinning, or electro-hydraulic forming, the mechanical properties and forming limits of high-purity niobium sheets must be measured. Both quantities are used in finite element (FE) models of the forming operations to predict the final geometry of the cavity and the risk of occurrence of necking (failure). The mechanical properties at low strain rates are easily obtained by performing standard tensile tests (ASTM E8 [5] or ISO 6892-1:2016 [6]) and anisotropic properties are measured by testing specimens cut in the sheets at 0 deg, 45 deg, and 90 deg angles, with respect to the rolling direction. Determining the forming limit diagram (FLD) of a material is much more complicated and expensive.

An FLD is a useful tool to predict the formability of a sheet metal for different forming conditions, from uniaxial tension to balanced biaxial stretching. Sheet formability was first extensively studied by Keeler [7] and experimental techniques to obtain FLDs are now

[1]Corresponding author.
Contributed by the Materials Division of ASME for publication in the Journal of Engineering Materials and Technology. Manuscript received February 1, 2021; final manuscript received August 13, 2021; published online October 21, 2021. Assoc. Editor: Philip Eisenlohr.

standardized [8]. The Nakajima (out-of-plane) and Marciniak (in-plane) [9,10] tests have been widely used to obtain the FLDs of materials at different temperatures and strain rates. Only one forming limit diagram was found in literature for niobium. Daumas and Collard [11] performed Nakajima tests against pressurized oil on 1 mm and 2 mm thick sheets. However, the forming limit curves (FLCs) only spanned for minimum and maximum minor strains of about −0.1 and 0.1, respectively. The low value of 0.1 for the maximum minor strain was likely caused by important friction forces between the punch and the sheet, and this could be optimized to increase the sheet formability.

The objectives of this study are twofold. First, the experimental forming limit diagram of high-purity niobium is obtained to update the only data found in the literature following advancements in high-purity niobium sheet manufacturing. Second, a model for the niobium formability is proposed. This model, based on the two-zone approach, was identified from the experimental data (obtained at a quasi-static strain rate in the order of 10^{-3} s^{-1}) and is used to evaluate the formability at high strain rates (up to 10^{4} s^{-1}) for high-speed sheet forming, such as electro-hydraulic forming. Lessons learned to design blank carriers that yield valid tests are also presented.

2 Experimental Procedures

The forming limit diagram of high-purity niobium, with a RRR of ∼363, was obtained by measuring the major and minor strains at the onset of localized necking for different strain paths, as specified in the ISO 12004-2:2008 standard [8]. The niobium sheets were manufactured by Ningxia Orient Tantalum Industry Co., Ltd. by multiple forging, rolling, and annealing steps, following the production of a high-purity ingot by electron beam melting [12–14]. The last two steps of the process were an annealing heat treatment, to reach complete recrystallization, and sheet leveling to ensure that thickness and flatness tolerances were respected. The Marciniak (in-plane) tests, with a 75 mm diameter flat-bottomed brass punch, were performed on rectangular blanks with a thickness of 1 mm, a constant length of 200 mm, and widths of 80, 100, 120, 140, 150, and 180 mm. A schematic of the cross section of the punch used for the Marciniak tests is presented in Fig. 1. Negative minor strains ($\varepsilon_2 < 0$) were measured for blanks with a width lower or equal to 120 mm and positive minor strains ($\varepsilon_2 > 0$) were measured for larger blanks. To force the failure of the niobium blanks to occur over the flat region of the punch instead of the punch radius, blank carriers are used in Marciniak tests [8]. Sheets of annealed (600 °C in vacuum for 2 h) oxygen-free electronic (OFE) copper with a thickness of 1 mm were used as blank carriers. The blank carrier and blank were held between an open die and a blank holder to restrict draw-in. A load of 170 kN was applied on the blank holder with a mechanical press and six screws were used to hold the die–blank holder assembly together. Two half-length sheets were used as blank carriers for the 80, 100, and 120 mm wide sheets and pierced sheets with a centered hole with a diameter of 30 mm was used for the wider sheets. The hole diameter was selected based on a preliminary study on annealed OFE copper (which is less expensive than niobium) for different hole diameters of 5 mm–30 mm [15]. The effect of friction was also studied with OFE copper blanks by using a 200 μm polyvinyl chloride (PVC) film and a 50 μm polytetrafluoroethylene (PTFE) film between the brass punch and the copper blank carrier [15]. For this study on niobium, only PTFE films were used.

In addition to the Marciniak tests, tensile tests with two different specimen geometries were performed. First, a standard tensile specimen with a uniaxial stress state and a geometry based on the ASTM E8 standard [5] was used. Second, a specimen with a short and wide gage length for near plane-strain deformation, based on the geometry used by Xavier et al. [16], was used. The tensile tests were performed at a constant cross-head speed of 5 mm/min, corresponding to a nominal strain rate of $\sim 1.08 \times 10^{-3}$ s^{-1} for the uniaxial test. Sheets with both geometries were cut at angles of 0 deg, 45 deg, and 90 deg between the loading and rolling directions to characterize the plastic anisotropy of the sheets. Figure 2 shows the different specimen geometries used in this study and their main dimensions.

All tests were performed until failure and pictures of the flat surface of the blank were acquired during the tests with a charge-coupled device camera (Pike) at two frames per second. A mirror was placed above the blank and angled at 45 deg to install the camera away from the mechanical press. Before testing, the specimens were painted with a thin uniform white matte layer and a stochastic pattern was applied with black paint. The stochastic pattern was used in a digital image correlation (DIC) software (GOM Correlate) to measure the strain field in the niobium blank. The true (logarithmic) minor and major strains were calculated with the DIC software and extracted for each frame at five points on either side of the neck to plot the strain path of each test. The points of the forming limit curve were calculated using a MATLAB code developed by the authors to fit the major strain data of a linear scan perpendicular to the neck following the method proposed in the ISO standard [8]. The frame selected for the analysis was based on the visual observation of light reflections on the niobium blank due to a rupture of the paint. The rupture of the paint in the necked region was caused by a rapid increase in strain and DIC analysis confirmed that the observation of these reflections occurred during localized necking. The accuracy of this method was verified in a previous study of the authors with annealed OFE copper (unpublished) by comparing the experimentally obtained FLC with results from the literature for a similar high-purity grade copper and with independent analyses done by two users using different DIC software packages.

The plastic strain anisotropy coefficients, also called r-values or Lankford coefficients, were calculated using the uniaxial tensile tests with their tensile axis at 0 deg, 45 deg, and 90 deg with respect to the rolling direction. The manual method specified in the ASTM E517 standard [17] was used with digital image correlation. The change in axial length in the gage section from an initial length (L_0) of approximately 50 mm was measured at true strains of 0.15 and 0.20. The transversal change in width for an initial width (w_0)

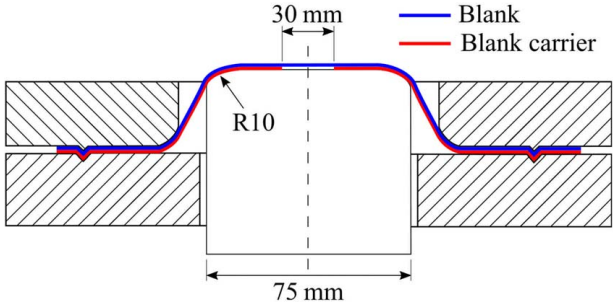

Fig. 1 Schematic of the Marciniak punch with a deformed blank and blank carrier and important dimensions (not to scale)

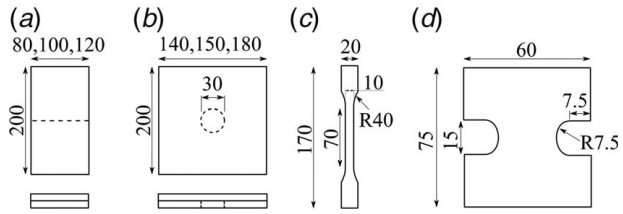

Fig. 2 Schematic of the different blank geometries (not to scale and with dimensions in mm) used to obtain the FLC of high-purity niobium for (*a*) and (*b*) Marciniak, (c) uniaxial tensile, and (*d*) plane-strain tests

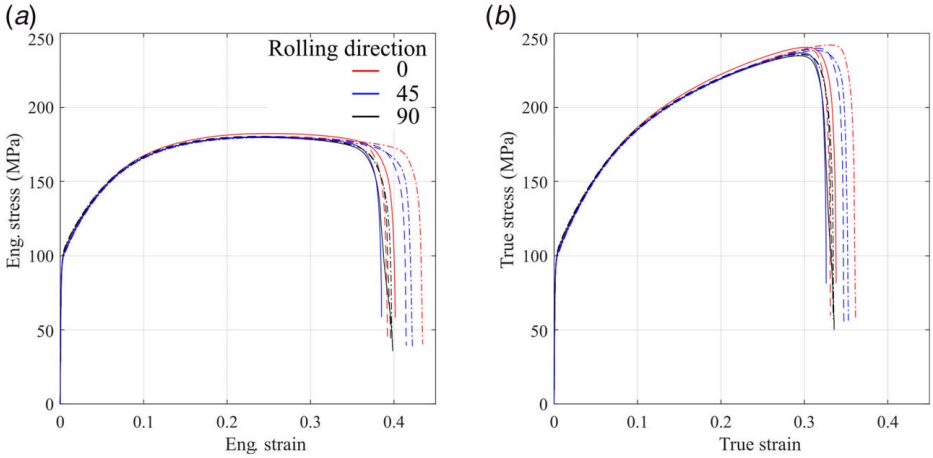

Fig. 3 (*a*) Engineering and (*b*) true tensile mechanical properties of high-purity niobium polycrystalline sheets at a nominal strain rate of $\sim 1.08 \times 10^{-3}\ s^{-1}$ for different rolling directions. Dashed and dash-dotted lines are repetitions of tests with the same rolling direction.

of approximately 10 mm, averaged over three different regions of the specimen was also measured at the same strains. The final lengths (L_f) and widths (w_f) were used in the following equation to calculate the r-value for each rolling direction and value of true strain

$$r_\theta^\varepsilon = \frac{\ln\left(\frac{w_0}{w_f}\right)}{\ln\left(\frac{L_f w_f}{L_0 w_0}\right)} \tag{1}$$

where ε represents the true strain at which the r-value is calculated ($\varepsilon = 0.15$ or $\varepsilon = 0.20$) and θ represents the angle, in degree, between the rolling direction and the tensile axis of the specimen ($\theta = 0$ deg, $\theta = 45$ deg, or $\theta = 90$ deg).

The weighted average r-value of high-purity niobium was calculated at each level of strain using the following equation:

$$r_m^\varepsilon = \frac{r_0^\varepsilon + r_{90}^\varepsilon + 2 \times r_{45}^\varepsilon}{4} \tag{2}$$

and the degree of planar anisotropy was calculated with the following equation:

$$\Delta r^\varepsilon = \frac{r_0^\varepsilon + r_{90}^\varepsilon - 2 \times r_{45}^\varepsilon}{2} \tag{3}$$

3 Results and Discussion

3.1 Tensile Mechanical Properties of Niobium Sheets. Figure 3 shows the uniaxial tensile properties of high-purity niobium specimens cut in different orientations. The stress–strain curves show that the niobium sheets have similar mechanical properties in the different loading directions. The low variation in yield stress and ultimate tensile strength reported in Table 1 support the observation made from the stress–strain curves. The mean yield stress and ultimate tensile stress (UTS), using a formulation analogue to the one used in Eq. (2) to calculate the mean plastic strain anisotropy, are equal to 98.52 MPa and 180.20 MPa, respectively.

Table 1 also presents the engineering strain at UTS and the post-uniform elongation (the difference between the engineering strain at failure and at UTS). The post-uniform elongation is similar for all sheet rolling directions and rather large, with an average value of 0.16. Note that the post-uniform elongation is highest for materials with a large strain rate sensitivity such as niobium (the strain rate sensitivity exponent m of the present high-purity niobium is about 0.112 [18]). Ghosh [19] reported a monotonically increasing dependence between post-uniform elongation and the strain rate sensitivity exponent m, explained by hardening of the necked region of the specimen due to a local increase in strain rate.

An average hardening coefficient n of 0.236 has been found for the stress–strain curves of Fig. 3. Note that a power law constitutive equation, such as the Hollomon equation ($\sigma = K\varepsilon^n$, where K is a material constant), is not appropriate for niobium since the strain rate sensitivity is not considered and a more complex hardening function is required (see Sec. 4). However, the value of n is reported to allow comparisons with different materials, such as aluminum, steel, and brass in Fig. 8 of Gosh [19].

Table 2 shows the calculated plastic anisotropy values for the different tensile directions and the mean value r_m at true strains of 0.15 and 0.20. Since the difference is negligible between the two levels of strain, the average value is calculated and used. Those results show that high-purity niobium sheets have anisotropic plastic properties and a higher resistance to thinning in the 0 deg and 90 deg directions, i.e., $r_{0,90} > 1$. A high r_m generally enhances the drawability of the sheet, but a nonzero degree of planar anisotropy Δr indicates that earing and other shape defects are expected during the forming process [20].

3.2 Strain Paths and Forming Limit Diagram. Figure 4 shows the strain paths measured on either side of a neck in

Table 1 Tensile mechanical properties at yield and at the maximum load for all rolling directions

Rolling direction (deg)	0.2% yield (MPa)	UTS (MPa)	Eng strain at UTS (dimensionless)	Post-uniform elongation (dimensionless)
0	98.60	180.98	0.25	0.16
90	100.35	180.05	0.24	0.16
45	97.56	179.89	0.25	0.16

Table 2 Plastic anisotropy coefficients (r-values) of niobium for different rolling directions and strain levels

r_θ^ε	$\varepsilon = 0.15$	$\varepsilon = 0.20$	Average
$\theta = 0$ deg	1.67	1.66	1.66
$\theta = 90$ deg	2.30	2.30	2.30
$\theta = 45$ deg	1.00	0.99	1.00
r_m	1.49	1.49	1.49
Δr	0.982	0.986	0.984

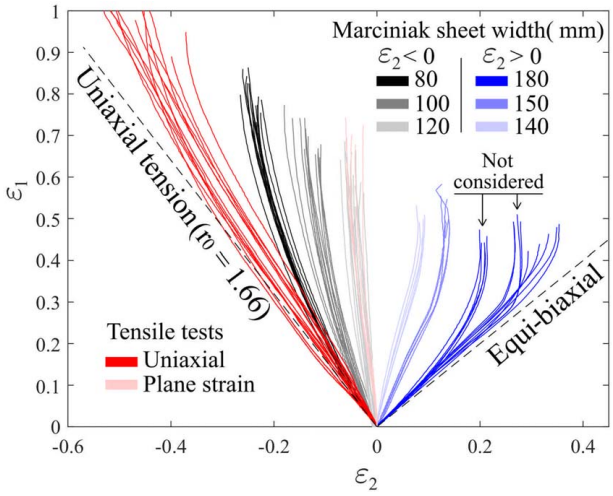

Fig. 4 Strain paths of the Marciniak and tensile tests for niobium sheets with the major strain aligned with the 0 deg rolling direction

Marciniak and tensile test specimens. Since the measurements are taken close to the neck and for frames beyond the onset of localized necking, the last points of the strain path in this figure are higher than the forming limit curve shown in Fig. 5. Dashed lines are also plotted to present the theoretical strain paths for (1) uniaxial tensile tests, based on the mean *r*-value of 1.66 for the 0 deg orientation, and (2) equi-biaxial tension. As expected, the strain paths of the Marciniak tests are all between those boundaries. At least three specimen geometries yielded results with negative and positive minor strains, which ensures that the FLC is representative of the material in all regions of the major strain–minor strain plot.

As shown in Fig. 4, the strain paths for tests with negative minor strains ($\varepsilon_2 < 0$) are all fairly linear from the beginning of the test up to necking, as required by the ISO 12004-2:2008 standard [8]. For wider sheets with strain paths with positive minor strains ($\varepsilon_2 > 0$), the bilinear strain path due to a failure of the blank carrier before the niobium blank is visible in few instances for sheets with widths of 150 mm and 180 mm. After inspection of the DIC results and the load versus punch displacement curves, the blank fails only few frames after the failure of the blank carrier for the 150 mm × 200 mm sheet, which limits the impact of the biaxial prestraining on the forming limit curve. For the 180 mm × 200 mm sheets, the change in strain path appears to be more important. Those specimens, identified in Fig. 4, were then not considered in the elaboration of the FLC as underestimation of the forming limit diagram are expected for tests with highly nonlinear strain paths with an initial biaxial component [21].

Figure 5 shows the experimental points of the forming limit curve for all sheets aligned with the rolling direction parallel to the major strain axis for the Marciniak tests and tensile tests in the longitudinal (0 deg) direction. The points with a negative minor strain show a linear trend with a negative slope. However, the leftmost points corresponding to the uniaxial tensile tests are higher than the straight dashed line plotted based on the mean plastic strain anisotropy value in the rolling direction calculated using the same specimens. A major strain difference of approximately 18% was calculated by taking the difference in major strain between the dashed line and the determined point of the FLC, at the minor strain value calculated for the FLC. This difference is likely caused by the slightly nonlinear strain path (Fig. 4), which could be due to the failure of the tensile specimens at approximately 45 deg. Human factors in the calculation of the *r*-values using DIC measurements, especially due to the high sensitivity to changes in width [17], could also affect the mean *r*-value. This difference shows the necessity of using a safety margin of about 10% [22] when using a FLC in finite element models to predict the formability of a part.

Similar (ε_2, ε_1) points were extracted from the plane-strain tensile tests in the longitudinal direction and the 120 mm × 200 mm sheets used in the Marciniak tests. This confirms that the nonstandardized near plane-strain tensile test used in this study is adequate to characterize the formability of the sheet metal for this strain state. The tensile test is much easier to perform than the traditional Nakajima and Marciniak tests. Only a standard tensile machine and one camera for 2D DIC are required. Problems associated with frictions are inexistent, the complex blank carrier design work is not required, and, therefore, it should easily be used for other materials. Xavier et al. [16] previously used this specimen geometry for interstitial-free and spheroidized SAE 1050 steels and compared the results of the near plane-strain tensile tests with Nakajima tests. Experimental results using both techniques and results from the literature confirm the efficacy of the near plane-strain tensile test to determine the lowest point of the FLC, called FLC_0.

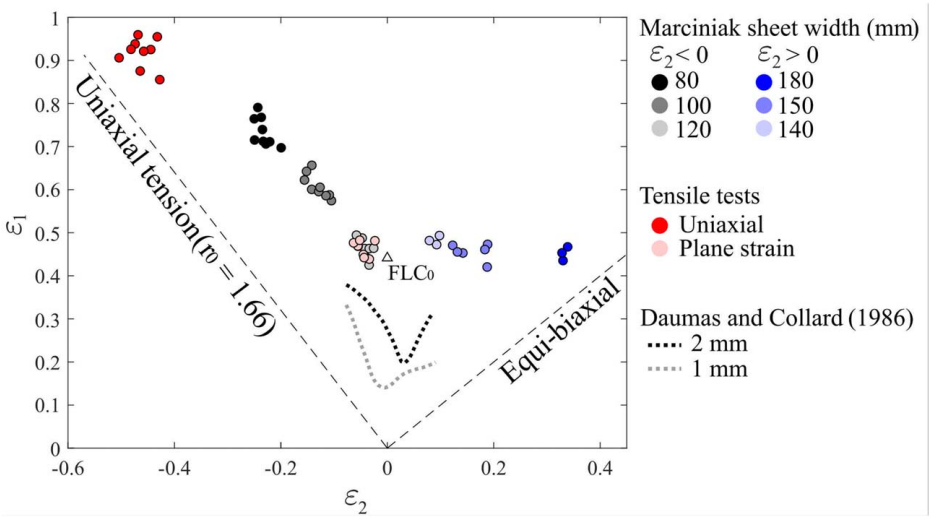

Fig. 5 Forming limit curve of high-purity niobium for sheets aligned with the rolling direction parallel to the major strain axis and an approximated value of FLC_0 for pure plane-strain deformation ($n = 0.236$ and $m = 0.112$). The experimental FLCs measured by Daumas and Collard [11] for niobium sheets with thicknesses of 1 and 2 mm are also presented for comparison with this study.

However, the FLC_0 point is often at $\varepsilon_2 = 0$ for materials with no pre-straining [23], like the high-purity niobium sheets used in this study. The points obtained from the near plane-strain tensile and Marciniak tests have average minor strains of −0.05 and −0.04, respectively. A linear extrapolation of the experimental data with negative minor strains was performed and the intersection of the major strain axis was found at a true strain of 0.44, which corresponds to an estimate of the formability limit for pure plane-strain deformation. A translation of the FLC_0 to a negative minor strain value is expected for uniaxial pre-straining [23,24]. However, the sheets were annealed by the manufacturer, which removed residual stresses from the rolling steps. The estimation of an FLC_0 at a minor strain of zero is then a reasonable estimate of the formability of the material. It is interesting to notice that all points with positive minor strains have approximately equal values of major strain. This finding is consistent with theoretical results reported by Marciniak et al. [25] for viscoplastic materials with a high strain rate sensitivity m (see Fig. 4 in Ref. [25] and recall that $m \sim 0.112$ for the present high-purity niobium [18]).

Finally, note that the obtained experimental results are very different than the FLCs obtained by Daumas and Collard [11] in 1986 for niobium sheets with thicknesses of 1 mm and 2 mm, see Fig. 5. The forming limit diagrams presented by those authors had much lower formability (lower ε_1) and narrower (smaller minimum and maximum ε_2) curves for sheets with equal or higher thicknesses. The large increase in formability in this study is likely caused by an increase in purity of niobium sheets from the manufacturers in the last three decades or to a more recrystallized microstructure with a lower initial dislocation density. This hypothesis is based on the difference in yield stress between the two studies. The yield stress measured by Daumas and Collard [11] was about twice as high as the sheets used in this study. The large difference in formability with the only FLD of niobium available in the literature confirms the objective of this article to provide an updated forming limit curve for high-purity niobium sheets used in SRF applications.

4 Modeling

This section deals with the modeling of the formability of the considered high-purity polycrystalline niobium using the two-zone model proposed by Jacques [26]. This model extends the classical Marciniak–Kuczyński [9] framework to include inertia effects (which may be important in the case of high-speed forming processes, such as electro-hydraulic forming). The presentation of this model is not repeated here as it is described in details in Ref. [26], see also Ref. [27] for the case of anisotropic materials. However, it is useful to mention that the model considers a thin sheet subjected to biaxial in-plane stretching. The evolution of the components of the overall deformation gradient in the main straining directions is given by

$$F_{11} = 1 + \dot{F}_{11} \cdot t \tag{4a}$$

$$F_{22} = 1 + \dot{F}_{22} \cdot t \tag{4b}$$

with $\dot{F}_{11} > 0$ and $-\dot{F}_{11}/2 \leq \dot{F}_{22} \leq \dot{F}_{11}$. The main straining direction 1 is assumed to coincide with the sheet rolling direction. Moreover, the model assumes an imperfection in the form of a zone of reduced thickness. The relative imperfection amplitude is $\xi = \dfrac{h_0^I - h_0}{h_0}$, with h_0^I and h_0 being, respectively, the values of the initial sheet thickness inside and outside the imperfection.

The anisotropic Hill 48 plasticity model [28] is adopted to describe the niobium behavior. Assuming plane-stress conditions, the yield function can be written as

$$f = [(G+H)\sigma_{11}^2 + (H+F)\sigma_{22}^2 - 2H\sigma_{11}\sigma_{22} + 2N\sigma_{12}]^{\frac{1}{2}} - \bar{\sigma} \tag{5}$$

where $\bar{\sigma}$ is the flow stress of the material in the rolling direction. The mechanical response of niobium exhibits a significant sensitivity to strain rate [18,29,30]. As strain rate sensitivity is known to have a significant effect on formability [19,25], it should be taken into account in the modeling. A common assumption of an additive decomposition of the flow stress into an athermal stress σ_a and a thermal (or thermally activated) stress σ_{th} was adopted [31]. In the case of BCC metals, it is admitted that the thermal stress is related to the existence of short-range barriers (the Peierls barriers) hindering the motion of dislocations. For this reason, the thermal stress is nearly independent of plastic strain [31–33]. Therefore, the flow stress of the material may be given as[2]

$$\bar{\sigma} = \sigma_a(\bar{\varepsilon}) + \sigma_{th}(\dot{\bar{\varepsilon}}) \tag{6}$$

where $\bar{\varepsilon}$ and $\dot{\bar{\varepsilon}}$ are the effective plastic strain and plastic strain rate, respectively. A mixed Swift-Voce relation is used to describe strain hardening (evolution of the athermal stress with plastic strain)

$$\sigma_a = \sigma_0[c(1 - \exp(-\alpha\bar{\varepsilon})) + d\bar{\varepsilon}^n] \tag{7}$$

where c, α, d, and n are material parameters and σ_0 is a reference stress. High strain rate experiments have revealed that the logarithmic strain rate sensitivity of niobium is almost constant (for strain rates up to $1600\ s^{-1}$) [18]. This suggests the use of a power law to evaluate the thermal stress

$$\sigma_{th} = \sigma_0 \left(\frac{\dot{\bar{\varepsilon}}}{\dot{\varepsilon}_r}\right)^m \tag{8}$$

The parameters related to strain hardening (c, α, d, and n) and the reference stress σ_0 have been identified from the results of the tensile tests presented in Sec. 3.1. The values of the orthotropy parameters (F, G, H, and N) have been determined from the r-values measured in the 0 deg, 45 deg, and 90 deg directions (Sec. 3.1). The strain rate sensitivity exponent m has been identified from results of the high strain rate tensile tests performed by Croteau et al. [18]. The material parameters are given in Table 3.

Figure 6 presents a comparison between the experimental measurements and the results obtained with the two-zone model for an imperfection amplitude of $\xi = 0.5\%$. This imperfection amplitude was chosen as it provides conservative estimates on formability for most loading paths. Overall, a fairly good agreement is observed. However, the model tends to overestimate necking strains for loading paths closed to balanced biaxial extension. To illustrate the role of the anisotropic properties of the niobium sheets on the formability, results obtained using the von Mises yield function are plotted in Fig. 6. Plastic anisotropy only affects the right side of the FLC. When anisotropy is not accounted for, larger discrepancies between modeling and experiments are observed. In Fig. 6, the FLC obtained when the strain rate

Table 3 Material parameters used in the formability analyses for niobium

Orthotropy parameters	F	0.271
	G	0.376
	H	0.624
	N	0.971
Reference stress	σ_0	93.15 MPa
Strain-hardening parameters	c	0.937
	α	12.6
	d	1.511
	n	0.65
Reference strain rate	$\dot{\varepsilon}_r$	$10^{-3}\ s^{-1}$
Strain rate sensitivity exponent	m	0.112
Mass density	ρ	$8570\ kg/m^3$

[2]Note that the thermal stress is also temperature dependent. However, in the present work, the influence of temperature on formability is not considered.

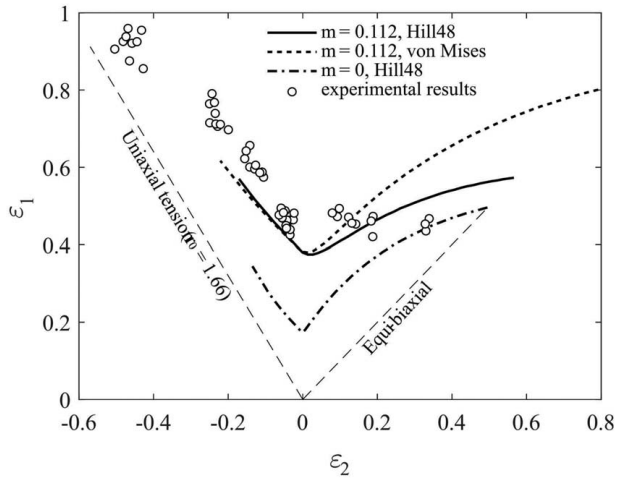

Fig. 6 Comparison between FLCs derived from the two-zone model and the experimental necking strains. The reference curve ($m = 0.112$, Hill 48) has been obtained with the material parameters given in Table 3 and an imperfection amplitude $\xi = 0.5\%$. The FLCs corresponding to an isotropic von Mises material ($F = G = H = 0.5$ and $N = 1.5$) and a rate-insensitive material ($m = 0$) are also presented. The principal initial strain rate is $\dot{F}_{11} = 10^{-3}\ s^{-1}$.

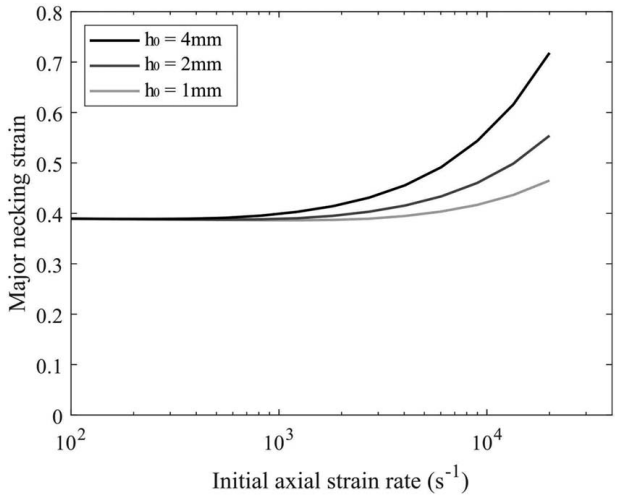

Fig. 7 Evolution of the major necking strain as a function of the initial axial strain rate $\dot{F}_{11}$ for several values of initial sheet thickness h_0. The loading conditions corresponds to plane-strain stretching ($\dot{F}_{22} = 0$) and the imperfection amplitude is $\xi = 0.5\%$.

sensitivity of niobium is neglected ($m = 0$ in Eq. (6)) is also displayed. In this case, the necking strains are underestimated by about 0.27 with the two-zone model. This result indicates that the rather high formability of niobium is related to its pronounced strain rate sensitivity.

As mentioned in Sec. 1, high-speed forming techniques can be used to produce SRF cavities. Therefore, it is of interest to investigate the influence of strain rate on the formability of niobium. Several studies have shown that the development of a neck at high strain rate can be delayed by inertia effects, leading to formability improvements [34–36]. Figure 7 displays the evolution of the necking strain for plane-strain deformation (corresponding to the lower point of the forming limit curve, FLC_0) as a function of the prescribed initial strain rate $\dot{F}_{11}$ for several values of initial sheet thickness. The results are presented for strain rates larger than $100\ s^{-1}$ as no significant necking strain variation are observed below. The results presented in Fig. 7 show that a significant increase in formability can be achieved at high strain rate. With the present modeling, the formability improvement is due to inertia effects. Under dynamic loading conditions, the development of necking can be impeded due to in-plane accelerations [37]. Therefore, larger strains can be reached before the occurrence of localized necking. As inertia effects are dependent on the sheet thickness (see Sec. 3.2 in Ref. [26]), the increase in ductility at high strain rate is more pronounced for thicker sheets. When the applied strain rate goes from $100\ s^{-1}$ to $10{,}000\ s^{-1}$, the necking strain increases by 9% for $h_0 = 1$ mm, 21% for $h_0 = 2$ mm, and 45% for $h_0 = 4$ mm. This shows that high-speed forming can be beneficial to SRF cavity manufacturing.

5 Conclusions

The forming limit diagram of high-purity niobium sheets used in the manufacturing of SRF cavities was obtained. Marciniak tests were performed at quasi-static strain rate in the order of $10^{-3}\ s^{-1}$ on niobium blanks with a thickness of 1 mm. Annealed OFE copper blank carriers with a thickness of 1 mm were used to force necking to occur over the flat region of the punch. Similar mechanical properties were measured from stress–strain curves in the 0 deg, 45 deg, and 90 deg directions with mean yield and ultimate tensile stresses of 98.52 MPa and 180.20 MPa, respectively. However, the plastic strain anisotropy coefficients of the high-purity niobium sheets were found to be dependent on the loading direction. r-values of 1.66, 1.00, and 2.30 were measured for the 0 deg, 45 deg, and 90 deg directions, respectively. A high formability was measured with all points of the FLC above a true major strain at necking of 0.42.

Theoretical calculations of the FLC with the two-zone model proposed by Jacques [26] were in agreement with the experimental results for most of the FLC and overestimated the formability near equi-biaxial strain. A comparison with results obtained with the von Mises model (isotropic material) and a rate-insensitive constitutive law indicates that both anisotropy and strain rate sensitivity affect the formability of niobium. The model was further used to evaluate the formability of niobium for dynamic loading conditions (representative of high-speed sheet forming operations). For thicker niobium sheets of up to 4 mm, an increase in major necking strain is expected at strain rates greater than $\sim 800\ s^{-1}$.

Finally, the experimental FLC measured at a quasi-static strain rate ($\sim 10^{-3}\ s^{-1}$) in this study should be compared with future experimental measurements at strain rates closer to the forming condition during electro-hydraulic forming, i.e., at around $10^3\ s^{-1}$ to $10^4\ s^{-1}$.

Acknowledgment

This Marie Sklodowska-Curie Action (MSCA) Innovative Training Network (ITN) receives funding from the European Union's H2020 Framework Programme under Grant Agreement No. 764879.

Conflict of Interest

There are no conflicts of interest.

Data Availability Statement

Data reported in the paper are available upon request to the corresponding author.

References

[1] Carra, F., Carvalho, A. A., Artoos, K., Atieh, S., Santillana, I. A., Boucherie, A. B., Brachet, J. P., et al., 2015, "Crab Cavity and Cryomodule Development for HL-LHC," SRF2015, pp. 1460–1467.

[2] Belomestnykh, S., and Shemelin, V., 2005, "High-β Cavity Design—A Tutorial," The 12th International Workshop on RF Superconductivity, Ithaca, NY, https://www.classe.cornell.edu/public/SRF/2006/SRF060424-03/SRF060424-03.pdf, Accessed January 20, 2021.
[3] Abada, A., Abbrescia, M., AbdusSalam, S. S., Abdyukhanov, I., Abelleira Fernandez, J., Abramov, A., Aburaia, M., et al., 2019, "FCC-ee: The Lepton Collider: Future Circular Collider Conceptual Design Report Volume 2," Eur. Phys. J. Spec. Top., **228**(2), pp. 261–623.
[4] Abada, A., Abbrescia, M., AbdusSalam, S. S., Abdyukhanov, I., Abelleira Fernandez, J., Abramov, A., Aburaia, M., et al., 2019, "FCC-hh: The Hadron Collider: Future Circular Collider Conceptual Design Report Volume 3," Eur. Phys. J. Spec. Top., **228**(4), pp. 755–1107.
[5] ASTM International, 2016, "ASTM E8/E8M-16ae1, Standard Test Methods for Tension Testing of Metallic Materials," http://astm.org, Accessed April 2, 2020.
[6] International Organization for Standardization, 2016, "ISO 6892-1:2016—Metallic Materials—Tensile Testing—Part 1: Method of Test at Room Temperature," https://www.iso.org/standard/78322.html, Accessed November 21, 2020.
[7] Keeler, S. P., 1961, "Plastic Instability and Fracture in Sheets Stretched Over Rigid Punches," Ph.D. thesis, Massachusetts Institute of Technology, Cambridge, MA. https://dspace.mit.edu/handle/1721.1/120282
[8] International Organization for Standardization, 2008, "ISO 12004-2:2008—Metallic Materials—Sheet and Strip—Determination of Forming-Limit Curves—Part 2: Determination of Forming-Limit Curves in the Laboratory," https://www.iso.org/standard/43621.html, Accessed March 30, 2020.
[9] Marciniak, Z., and Kuczyński, K., 1967, "Limit Strains in the Processes of Stretch-Forming Sheet Metal," Int. J. Mech. Sci., **9**(9), pp. 609–620.
[10] Raghavan, K. S., 1995, "A Simple Technique to Generate in-Plane Forming Limit Curves and Selected Applications," Metall. Mater. Trans. A, **26**(8), pp. 2075–2084.
[11] Daumas, M. T., and Collard, J., 1986, "Pure Niobium Sheet Formability Limits Hydroforming," The 14th International Deep Drawing Research Group Biennal (IDDRG-14), April.
[12] Saito, K., and Furuta, F., 2009, "Multi-Wire Slicing of Large Grain Ingot Material," The SRF2009, Berlin, Germany. https://accelconf.web.cern.ch/SRF2009/papers/thoaau05.pdf, Accessed April 15, 2020.
[13] Antoine, C., 2012, "Materials and Surface Aspects in the Development of SRF Niobium Cavities," DSM IRFU CEA Centre d'Etudes de Saclay, EuCARD-BOO-2012-001. http://cdsweb.cern.ch/record/1472363, Accessed April 24, 2018.
[14] Singer, W., 2015, "SRF Cavity Fabrication and Materials," CERN Yellow Rep. CERN-2014-005, pp. 171–207.
[15] Croteau, J.-F., 2021, "Single Crystal and Polycrystalline Niobium and OFE Copper for SRF Cavities Applications: Mechanical Characterization at Low to High Strain Rates and Microstructural Investigations," Ph.D. thesis, ENSTA Bretagne, Brest, France.
[16] Xavier, M. D., Plaut, R. L., and Schön, C. G., 2014, "Uniaxial Near Plane Strain Tensile Tests Applied to the Determination of the FLC0 Formability Parameter," Mater. Res., **17**(4), pp. 982–986.
[17] ASTM International, 2019, "ASTM E517-19, Standard Test Method for Plastic Strain Ratio r for Sheet Metal," http://astm.org, Accessed October 22, 2020.
[18] Croteau, J.-F., Peroni, M., Atieh, S., Jacques, N., and Cantergiani, E., 2021, "Effect of Strain Rate on the Tensile Mechanical Properties of Electron Beam Welded OFE Copper and High-Purity Niobium for SRF Applications," J. Dyn. Behav. Mater., **7**(3), pp. 485–492.
[19] Ghosh, A. K., 1977, "The Influence of Strain Hardening and Strain-Rate Sensitivity on Sheet Metal Forming," ASME J. Eng. Mater. Technol., **99**(3), pp. 264–274.
[20] Kalpakjian, S., and Schmid, S. R., 2014, *Manufacturing Engineering and Technology*, 7th ed., Pearson, Upper Saddle River, NJ.
[21] Geoffroy, J.-L., Goncalves, J., and Lemoine, X., 2007, "Adequately Used FLC's for Simulations," The International Deep-Drawing Research Group (IDDRG 2007), Győr-Hungary, May.
[22] Paul, S. K., 2013, "Theoretical Analysis of Strain- and Stress-Based Forming Limit Diagrams," J. Strain Anal. Eng. Des., **48**(3), pp. 177–188.
[23] Graf, A., and Hosford, W., 1993, "Effect of Changing Strain Paths on," Metall. Trans. A, **24A**(11), pp. 2503–2515.
[24] Barata Da Rocha, A., Barlat, F., and Jalinier, J. M., 1984, "Prediction of the Forming Limit Diagrams of Anisotropic Sheets in Linear and Non-Linear Loading," Mater. Sci. Eng., **68**(2), pp. 151–164.
[25] Marciniak, Z., Kuczyński, K., and Pokora, T., 1973, "Influence of the Plastic Properties of a Material on the Forming Limit Diagram for Sheet Metal in Tension," Int. J. Mech. Sci., **15**(10), pp. 789–800.
[26] Jacques, N., 2020, "An Analytical Model for Necking Strains in Stretched Plates Under Dynamic Biaxial Loading," Int. J. Solids Struct., **200–201**, pp. 198–212.
[27] N'souglo, K. E., Jacques, N., and Rodríguez-Martínez, J. A., 2021, "A Three-Pronged Approach to Predict the Effect of Plastic Orthotropy on the Formability of Thin Sheets Subjected to Dynamic Biaxial Stretching," J. Mech. Phys. Solids, **146**, p. 29.
[28] Hill, R., 1948, "A Theory of the Yielding and Plastic Flow of Anisotropic Metals," Proc. R. Soc. A, **193**(1033), pp. 281–297.
[29] Nemat-Nasser, S., and Guo, W., 2000, "Flow Stress of Commercially Pure Niobium Over a Broad Range of Temperatures and Strain Rates," Mater. Sci. Eng. A, **284**(1–2), pp. 202–210.
[30] Peroni, L., and Scapin, M., 2018, "Experimental Analysis and Modelling of the Strain-Rate Sensitivity of Sheet Niobium," EPJ Web Conf., **183**, p. 01014.
[31] Voyiadjis, G. Z., and Abed, F. H., 2005, "Effect of Dislocation Density Evolution on the Thermomechanical Response of Metals With Different Crystal Structures at Low and High Strain Rates and Temperatures," p. 45.
[32] Nemat-Nasser, S., and Isaacs, J. B., 1997, "Direct Measurement of Isothermal Flow Stress of Metals at Elevated Temperatures and High Strain Rates With Application to Ta and TaW Alloys," Acta Mater., **45**(3), pp. 907–919.
[33] Zerilli, F. J., and Armstrong, R. W., 1987, "Dislocation-Mechanics-Based Constitutive Relations for Material Dynamics Calculations," J. Appl. Phys., **61**(5), pp. 1816–1825.
[34] Balanethiram, V. S., and Daehn, G. S., 1992, "Enhanced Formability of Interstitial Free Iron at High Strain Rates," Scr. Metall. Mater., **27**(12), pp. 1783–1788.
[35] Daehn, G. S., Altynova, M., Balanethiram, V. S., Fenton, G., Padmanabhan, M., Tamhane, A., and Winnard, E., 1995, "High-Velocity Metal Forming—An Old Technology Addresses New Problems," JOM, **47**(7), pp. 42–45.
[36] Xue, Z., Vaziri, A., and Hutchinson, J., 2008, "Material Aspects of Dynamic Neck Retardation," J. Mech. Phys. Solids, **56**(1), pp. 93–113.
[37] Altynova, M., Hu, X., and Daehn, G. S., 1996, "Increased Ductility in High Velocity Electromagnetic Ring Expansion," Metall. Mater. Trans. A, **27**(7), pp. 1837–1844.